Grote, H. et al. (2016) High power and ultra-low-noise photodetector for squeezed-light enhanced gravitational wave detectors. Optics Express, 24(18), pp. 20107-20118.

http://eprints.gla.ac.uk/123292/

Deposited on: 24 August 2016

High power and ultra-low-noise photodetector for squeezed-light enhanced gravitational wave detectors

Hartmut Grote,[1,*] Michael Weinert,[1] Rana X Adhikari,[2] Christoph Affeldt,[1] Volker Kringel,[1] Jonathan Leong,[1] James Lough,[1] Harald Lück,[1] Emil Schreiber,[1] Kenneth A Strain,[3] Henning Vahlbruch,[1] and Holger Wittel[1]

[1]*Max-Planck-Institut für Gravitationsphysik (Albert-Einstein-Institut) and Leibniz Universität Hannover, Callinstr. 38, 30167 Hannover, Germany*
[2]*California Institute of Technology, Pasadena, CA 91125, USA*
[3]*SUPA, School of Physics and Astronomy, The University of Glasgow, Glasgow, G12 8QQ, UK*
[*] *hartmut.grote@ligo.org*

Abstract: Current laser-interferometric gravitational wave detectors employ a self-homodyne readout scheme where a comparatively large light power (5–50 mW) is detected per photo-sensitive element. For best sensitivity to gravitational waves, signal levels as low as the quantum shot noise have to be measured as accurately as possible. The electronic noise of the detection circuit can produce a relevant limit to this accuracy, in particular when squeezed states of light are used to reduce the quantum noise. We present a new electronic circuit design reducing the electronic noise of the photodetection circuit in the audio band. In the application of this circuit at the gravitational-wave detector GEO 600 the shot-noise to electronic noise ratio was permanently improved by a factor of more than 4 above 1 kHz, while the dynamic range was improved by a factor of 7. The noise equivalent photocurrent of the implemented photodetector and circuit is about $5\,\mu\mathrm{A}/\sqrt{\mathrm{Hz}}$ above 1 kHz with a maximum detectable photocurrent of 20 mA. With the new circuit, the observed squeezing level in GEO 600 increased by 0.2 dB. The new circuit also creates headroom for higher laser power and more squeezing to be observed in the future in GEO 600 and is applicable to other optics experiments.

References and links

1. B. P. Abbott *et al.*, "Observation of Gravitational Waves from a Binary Black Hole Merger," Phys. Rev. Lett. **116**, 061102+ (2016).
2. J. Appel, D. Hoffman, E. Figueroa, and A. I. Lvovsky, "Electronic noise in optical homodyne tomography," Phys. Rev. A **75**, 035802+ (2007).
3. K. L. Dooley, J. R. Leong, T. Adams, C. Affeldt, A. Bisht, C. Bogan, J. Degallaix, C. Gräf, S. Hild, J. Hough, A. Khalaidovski, N. Lastzka, J. Lough, H. Lück, D. Macleod, L. Nuttall, M. Prijatelj, R. Schnabel, E. Schreiber, J. Slutsky, B. Sorazu, K. A. Strain, H. Vahlbruch, M. Wąs, B. Willke, H. Wittel, K. Danzmann, and H. Grote, *et al.*, "GEO 600 and the GEO-HF upgrade program: successes and challenges," Classical and Quantum Gravity **33**, 075009+ (2016).
4. H. Grote, K. Danzmann, K. L. Dooley, R. Schnabel, J. Slutsky, and H. Vahlbruch, "First Long-Term Application of Squeezed States of Light in a Gravitational-Wave Observatory," Physical Review Letters **110**, 181101+ (2013).
5. The LIGO Scientific Collaboration, "Advanced LIGO," Classical and Quantum Gravity **32**, 074001+ (2015).
6. J. B. Johnson, "Thermal Agitation of Electricity in Conductors," Phys. Rev. **32**, 97–109 (1928).
7. P. Fritschel, M. Evans, and V. Frolov, "Balanced homodyne readout for quantum limited gravitational wave detectors," Optics Express **22**, 4224+ (2014).
8. The LIGO Scientific Collaboration, "A gravitational wave observatory operating beyond the quantum shot-noise limit," Nat Phys **7**, 962–965 (2011).
9. The LIGO Scientific Collaboration, "Enhancing the sensitivity of the LIGO gravitational wave detector by using squeezed states of light," Nature Photonics **7**, 613–619 (2013).

10. M. B. Gray, D. A. Shaddock, C. C. Harb, and H. A. Bachor, "Photodetector designs for low-noise, broadband, and high-power applications," Review of Scientific Instruments **69**, 3755–3762 (1998).

11. K. L. Dooley, E. Schreiber, H. Vahlbruch, C. Affeldt, J. R. Leong, H. Wittel, and H. Grote, "Phase control of squeezed vacuum states of light in gravitational wave detectors," Opt. Express **23**, 8235–8245 (2015).

12. D. V. Martynov *et al.*, "The Sensitivity of the Advanced LIGO Detectors at the Beginning of Gravitational Wave Astronomy," Phys. Rev. D **93**, 112004 (2016).

13. F. Seifert, "Resistor Current Noise Measurements," https://dcc.ligo.org/public/0002/T0900200/001/current_noise.pdf (2009)

14. G. Heinzel, "Electronic Noise in Interferometers," in: Gravitational Wave Detection II, Proceedings of the 2nd TAMA International Workshop on Gravitational Wave Detection, Tokyo October 19–22, *Universal Academy Press* Tokyo, Japan (1999)

1. Introduction

Gravitational waves have recently been detected for the first time, using ultra-sensitive laser interferometers [1]. These gravitational wave (GW) detectors, but also a number of other optics experiments, work in a regime where small, often transient, signals are to be detected on the background of instrument noise. For a large fraction of the sensitive frequency band the limiting instrument noise in GW detectors is shot noise associated with the quantized interaction of light fields with photodetectors. To optimize the overall sensitivity of a GW detector or other optics experiments of this kind, the inevitable shot noise should not be contaminated with other, avoidable, technical noise sources, as far as possible. **As *sensitivity* we define the minimum signal quantity that a device can measure at a given frequency. For GW detectors, this quantitiy represents the length change of interferometer arms. Speaking of a higher sensitivity is understood as a smaller minimum signal quantity that can be measured.** Often one would be satisfied with the notion that the shot noise somehow dominates other technical noise sources such as the noise of the photodiode electronics circuit. By how much shot noise should dominate is a matter of the application requirements: For some experiments it might be enough to have shot noise to equal the electronics noise (which is implicit in the notion of noise equivalent photocurrent or light power, as a reference point). For other experiments one may be satisfied whenever technical noise is a factor of a few below shot noise. For GW detectors, typically one tries to have technical noise sources a factor of 10 below the more fundamental noise sources, such as shot noise. A good reason for this is that GW detectors are expensive instruments of up to hundreds of million Dollars or Euros, such that when relating instrument sensitivity to cost, efforts to increase the sensitivity even by small amounts pay off quickly.

For squeezed light application the situation is even more severe, since in this case the shot noise is lowered by the squeezing factor. The observed squeezing of the shot noise can be limited by electronic noise though, a well known fact in squeezed light experiments. Seen from another perspective, it can be shown that electronic noise in the detection process of quantum states is equivalent to optical loss [2], and thus can limit the squeezing factor. Since the GEO 600 [3] gravitational-wave detector almost continuously uses squeezed states of light to lower the shot noise [4], a reduction of electronic noise in the PD readout was particularly sought, in order to gain the maximum benefit from squeezed light application.

Shot noise is the dominating noise source over a wide range of the GW detectors' frequency band, and thus mostly determines the sensitivity of the GW detector. Competing electronic noise that adds to the shot noise reduces the sensitivity. The sensitivity loss (or noise floor increase), as function of signal-to-noise ratio (SNR) of shot noise to competing electronic noise, can be expressed as $S_{loss} = \sqrt{1 + (1/\mathrm{SNR})^2} - 1$. Note that we regard shot noise as the 'signal' here, and do so throughout the paper.

It is a particular feature of GW detectors to measure the *amplitude* of GWs, **which decreases linearly with distance from the source.** Therefore, the *volume* in which astrophysical sources are detectable increases with the third power of **the GW detectors' range, and thus**

with the third power of the linear sensitivity. This holds for astrophysical sources within the relevant frequency band and assuming homogeneous distribution of sources in the volume. Therefore, the loss of sensitive volume, or event rate, as function of SNR can be expressed as $V_{loss} = \sqrt{1 + (1/\text{SNR})^2}^3 - 1$. Figure 1 shows V_{loss} and S_{loss} as function of SNR.
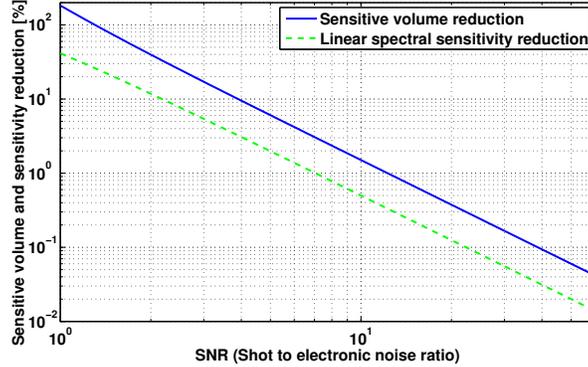

Fig. 1. Loss of sensitive volume to gravitational waves and loss of spectral sensitivity as function of the ratio of shot noise to electronic noise, or any other competing noise source. For a noise source a factor 4 below shot noise, the sensitive volume is reduced by almost 10 %. For a noise source a factor 10 below shot noise, the reduction in volume is 1.5 %.

For the electronic noise of the optical GW readout the goal to have electronic (readout) noise a factor 10 below shot noise has hardly been achieved in the past. In GEO 600 a factor of 7 was achieved (see Fig. 7) and for LIGO [5] a factor of 8 was achieved [12] at 100 Hz. However, even with a SNR of 10, the loss in sensitive volume would still be 1.5 %.

In this paper, we analyze the limitations of the current circuit design approach (section 2), identify ways to overcome these (section 3) and report on the successful application of a new detection circuit design at the GW detector GEO 600 (section 4). **Our solution is applicable to other optics experiments which measure quantum noise in the audio-band with high precision. An example are novel laser-amplitude stabilisation schemes using squeezed states of light.**

2. Existing solutions and their limitations

If operated with sufficient bias voltage, a photodiode (PD) linearly converts light power to electrical current, the latter denoted as *photocurrent* as a reminder of its origin. Further processing involves the conversion of the photocurrent I to a voltage U which is the quantity most conveniently used for re-distribution in analogue information processing systems. Photodetector circuits often (an exception are resonant detectors for radio frequencies) use an Ohmic resistor (called conversion resistor R below) for this current to voltage conversion, as visualized in Fig. 2.

We can analyze the associated signal-to-noise ratio of the I to U conversion with a conversion resistor R as follows: The (un-squeezed) shot noise amplitude spectral density $\tilde{I}_s$ of the photocurrent is

$$\tilde{I}_S = \sqrt{2eI} \tag{1}$$

with e being the elementary charge, and I the average current through the photodiode, resulting from detected photons (i.e. the photocurrent).

The current amplitude spectral density $\tilde{I}_T$ due to Johnson [6] noise of the resistor R is given by
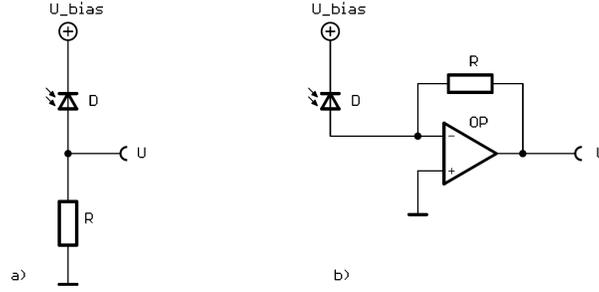
Fig. 2. Photodetection scheme with a photodiode D and current to voltage converting resistor R. Figure (a) (left) shows the most simple scheme. Figure (b) (right) shows a scheme with the resistor R in the feedback of an operational amplifier (also called *transimpedance* configuration), which has typically a larger range than the most simple scheme at the cost of additional noise from the opamp. Range limitations in both schemes come from the voltage across resistor R: Solution (a) is range limited as the effective bias voltage across the PD (D) is reduced when the voltage across R increases. Solution (b) is range limited by the maximum (negative) output voltage or current of the operational amplifier.

$$\tilde{I}_T = \sqrt{\frac{4k_B T}{R}} \tag{2}$$

with k_B being Boltzmann's constant and T the temperature of resistor R. We can now define the signal-to-noise ratio we want to maximize as

$$\text{SNR} = \frac{\tilde{I}_S}{\tilde{I}_T}. \tag{3}$$

As noted above, we view the shot noise spectral density as our signal of interest here. Inserting (1) and (2) into (3) yields

$$\text{SNR} = \sqrt{\frac{eIR}{2k_B T}}. \tag{4}$$

Obviously, the SNR can be increased by increasing the photocurrent I (and thus the detected light power) or the resistor R. However, this only goes so far, as one will hit range limitations from the electronics: The photocurrent I flowing across the conversion resistor R will produce a voltage $U = IR$ across the resistor, which has to be handled by the circuit. Substituting for IR yields

$$\text{SNR} = \sqrt{\frac{eU}{2k_B T}}. \tag{5}$$

It is now more clear that it is the maximum *voltage* across the sensing resistor which is the basic limitation, but not the photocurrent or the conversion resistor individually. For a given circuit with a maximum voltage U, an increase in photocurrent I could only be handled by a proportional decrease of R, thus nullifying any gain in SNR. An analogous result has been reported in [7] where the technique of balanced homodyne detection was mentioned as one means to lower the detection noise in the presence of squeezing. As we demonstrate in this paper, other means to lower the detection noise exist as well.

Equation (5) shows that there are two relevant limitations to the SNR: The voltage U across the conversion resistor and the temperature of that resistor. For the example of $U = 10\,\text{V}$ and

$T = 300\,\text{K}$ we obtain SNR $= 13.9$. Note however, this is an upper limit, which neglects other noise sources in the detection electronics such as amplifier noise and Johnson noise from other circuit resistors. The goal of a good circuit design would be to keep these other noise sources still further below the thermal noise of the conversion resistor.

Another factor reducing the SNR that can be achieved in practice, is that it is not desirable to operate the circuit at the limit of maximum sustainable voltage across the conversion resistor. Ultimately all circuit designs will allow a maximum voltage above which the circuit would become non-linear and saturate. To allow a safe operation under varying conditions (e.g. different possible power levels of light on the photodetector) one would often want to leave a margin of factor 2 or 3.

Figure 3 shows three curves according to Eq. (5). The solid curve reflects the SNR at room temperature as function of voltage across the conversion resistor for un-squeezed shot noise. GW interferometers to date achieve SNRs between 6 and 9 at best, corresponding to voltages of approx. 2 to 4 V (neglecting other noise sources).
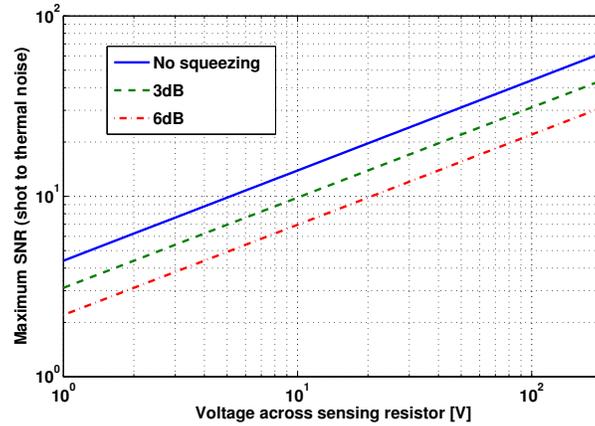

Fig. 3. Shot noise to thermal noise ratio as function of voltage detected across the (current to voltage) conversion resistor. Curves are computed according to Eq. (5) with $T = 300\,\text{K}$. For the lower two curves an assumed squeezing of the observed shot noise at the denoted levels is assumed, thus reducing the SNR and making the influence of electronic noise larger.

If squeezed vacuum states are injected into the GW detector, the remaining SNR (of shot noise to electronic noise) will be lower by the level of observed squeezing [8, 9]. To reach a SNR of 10 in the presence of 6 dB of squeezing observed, one would need to use a voltage across the conversion resistor of more than 20 V; including practical margins more like 60 V. Also, in this case the full photocurrent flows through the conversion resistor, leading to heat dissipation and potentially increasing flicker noise [13]. Whether these problems are solvable is subject to further investigation.

Another approach to increase the SNR, motivated by Eq. (5), would be to lower the temperature T of the conversion resistor R, as is practiced in other fields of ultra low-noise sensing such as radio astronomy. However, cooling R would be a significantly more complex solution. The sensing electronics are located inside the vacuum system for noise reasons, in the example of LIGO. Adding cryogenic operation to this would be a major intervention. To reach the same improvement as going from 10 V to 60 V operation, one would need a factor of 36 in temperature reduction, namely $T \approx 8\,\text{K}$. This is not trivial, also considering the heat load on the conversion resistor.

In the following we look at a different approach, which is to make the current to voltage

conversion a function of frequency, such that the low-frequency (or DC) component of the photocurrent would see a lower conversion impedance than the photocurrent at higher frequencies, in particular in the (nearly) shot noise limited band above 100 Hz. With this approach one can avoid using a high voltage and heat dissipation at the conversion resistor R. **Note that this approach makes use of the fact that the maximum voltage U required at the output of the conversion stage is determined by the DC component of the photocurrent. Therefore, if the conversion factor for the DC component can be reduced, the conversion factor for the band of interest can be increased without increasing the maximum voltage U. Another solution to reduce the effective DC conversion factor would be to subtract the DC component of the photocurrent before it enters the conversion resistor. This solution is problematic though for noise reasons, since it is very hard to construct a sufficiently low-noise current source.**

3. The new design

3.1. Circuit topology

An obvious and simple solution to make the current to voltage conversion frequency dependent would be to use an inductor instead of an ohmic resistor as conversion element. A solution of this kind is depicted in Fig. 4 (a). A resistor R in parallel to the inductor L is used to create a pole and flatten the frequency response above the pole frequency. At the pole frequency the reactive part of the impedance of L is equal to R and is given by $Z = 2\pi f L$. As an example, for an impedance of $10\,\text{k}\Omega$ at $f = 100\,\text{Hz}$ we would need an inductance of $L = 16\,\text{H}$. Since this is a rather large inductance, we evaluated electronic alternatives like gyrator circuits resembling the behavior of real inductors. While these circuits would be significantly more compact than a real inductor of several henry, we were not successful in finding any gyrator circuit that would have a sufficiently low noise current for our application. Note that the current noise spectral density of the conversion resistor (or general impedance for that matter) directly competes with the shot noise spectral density of the photocurrent. We therefore tried real impedances (i.e. coils), but in a slightly modified topology.

Figure 4 (b) shows a modification of Fig. 4 (a) in which the inductor L is not directly used as the current-to-voltage conversion element, but to act as frequency dependent impedance affecting the distribution of the photocurrent: At low frequencies most of the photocurrent I flows through inductor L to ground, whereas at high frequencies (i.e. in the audio band where we want the best SNR), most of the photocurrent flows towards the opamp where it is converted to a voltage across resistor R in the transimpedance configuration. A circuit with this topology has been described in Gray [10], though for application above the audio frequency band. **The novelty of the design suggested here lies in the fact that an adaption to audio frequency is developed, which hinges on the availability of suitable inductors for low-noise applications, as detailed below.**

Resistor R_i in Fig. 4 (b) is required in order to prevent the photocurrent from flowing through the transimpedance stage at low frequencies anyway, but it is also conveniently used to set the pole of the frequency response. Note that this topology has some similarity with the topology (a), but the final current to voltage conversion happens at resistor R in the feedback of the operational amplifier. An advantage of topology (b) is, that the inductance of inductor L can be reduced compared to topology (a), for the same pole frequency and (I to U) conversion factor. This is the case because R_i and R can be chosen independently, and thus the inductance L can be reduced by the factor R/R_i. A downside of topology (b) is however, the addition of noise from the operational amplifier and from resistor R_i. Effectively, this sets a practical limit on how low inductor L can be chosen: If L and R_i are too low, then the voltage noise of the operational amplifier becomes the dominant noise source within the audio band.

The actual solution finally tested and implemented in GEO 600 is shown in Fig. 9 in the appendix.
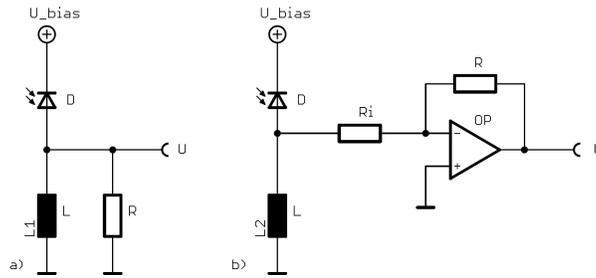
Fig. 4. Illustration of the alternative configurations using a frequency dependent impedance (an inductor in this case). Figure (a) (left) shows the simplest implementation. Figure (b) (right) shows a variant which allows for the independent tuning of corner frequencies of the response function at the cost of some additional noise from the operational amplifier.

3.2. Noise simulation

Figure 5 shows the simulated total electronic noise of the circuit tested in GEO 600 at the output X3 in Fig. 9. The simulation tool LISO [14] was used for this purpose. All components of the
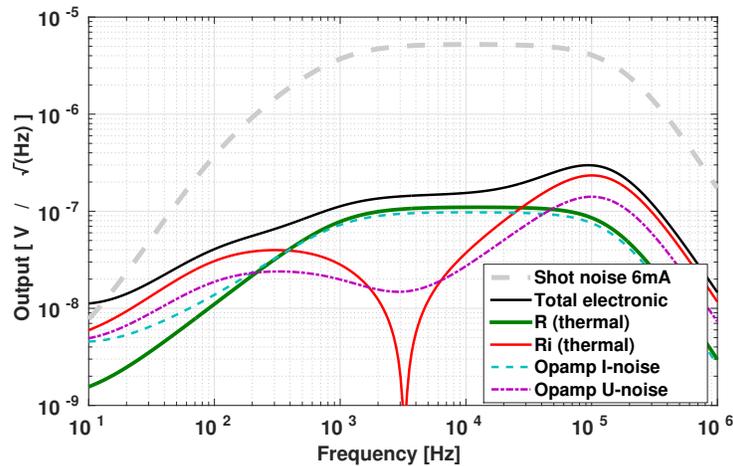
Fig. 5. Simulated noise at the output X3 of the tested circuit as shown in Fig. 9. The total electronic noise and the most relevant noise sources are shown. Shot noise from 6 mA of photocurrent is shown for comparison. See text for tedails. The simulation was done with LISO.

circuit are included in the noise model, but only the dominant or most interesting ones are shown in Fig. 5. The thermal noise of the current to voltage conversion resistor R dominates the total noise from about 400 Hz to 30 kHz. Below 400 Hz, the resistor Ri dominates the noise. To further reduce the contribution of resistor Ri one can increase the inductance of L2. Reducing Ri also lowers the contribution from Ri, but increases the contribution from opamp voltage noise. Also shown is the expected shot noise from a photocurrent of 6 mA, to illustrate the expected SNR as function of frequency. The choice of TLE2027 for the opamp is seeking a compromise between current and voltage noise. The contribution from the opamp current noise is close the the thermal noise of R, such that an opamp with lower current noise (such as an opamp with field-effect transistor input stage) could further reduce the noise of this circuit. The notch-like structure in the noise contribution from Ri and the opamp voltage noise come from the fact that the capacitance

of the photodiode PD (600 pF) and the inductor L2 (2 H) form a resonance circuit around 3 kHz. Seen from the direction of Ri, the resonance circuit has the highest impedance on resonance, such that noise current from Ri and opamp voltage noise are minimal at this frequency. Note that this resonance does not show up in the transfer function for the photocurrent.

3.3. Inductor core material

The largest problem to solve using this circuit design was to find a suitable core material for the inductor L. In order to achieve a high inductance, a ferro-magnetic core material seems appropriate to reduce the size of the coil in the first place. We tested several core materials (among them silicon-iron, SiFe) which showed problems with Barkhausen noise: In a test setup we applied a DC current of I=20 mA with a sinusoidal modulation of 1 mA (peak-to-peak) at 2.5 Hz, to simulate realistic fluctuations of the photocurrent. Under this condition, we measured glitches leading to an increase of the noise in the frequency domain (averaged over several seconds) of at least a factor of 10 at 100 Hz. Glitches were also observed when testing the circuit with the silicon-iron inductor at GEO 600, where a fluctuation of a few % of the detected light power frequently occurs on approx. second-long timescales.

The only core material yielding no glitches was mu-metal. Figure 6 shows noise measurements (under the test condition) of two inductors with different core material, namely SiFe and mu-metal.
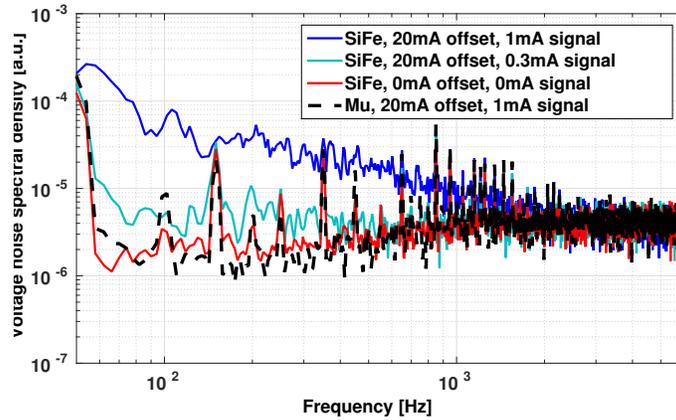

Fig. 6. Noise spectra for test conditions of two inductors. Offset current through the inductors and signal (sinusoidal modulation of the current) were applied as indicated. When a signal was applied to the coil with the SiFe core, excess noise was observed compared to the condition without signal, whereas no excess noise was observed for the mu-metal core. The excess noise was interpreted as Barkhausen noise.

The left hand side of Fig. 10 in the appendix shows images of the two inductors used for the measurements in Fig. 10. Both inductors were custom-made by EA Sowter Ltd in the UK. In order to minimize magnetic pickup by the inductor, we used shielding by a custom-made Mu-metal enclosure, also made by EA Sowter Ltd, for the inductor as shown in the right hand side of Fig. 10. The shielding reduced magnetic field pickup by about a factor of about 100 at frequencies around 100 Hz.

4. Experimental demonstration at the gravitational wave detector GEO 600

Before implementing the new readout electronics, GEO 600 was operating with a design, the *old* design, based on a single transimpedance stage as depicted in Fig. 2 (b). Under regular operating

conditions with 6 mA of photocurrent, the voltage across the resistor R in that circuit was 6 V. The maximum range was 12 mA of photocurrent, such that this circuit used 50 % of its range. The 6 V across resistor R corresponded to a maximum possible shot noise to electronic noise ratio of about factor 10 (without squeezing). A factor 7 was achieved in practice, mostly due to additional noise from operational amplifiers.

We then implemented the new circuit as depicted in Fig. 9. Figure 7 shows noise spectral densities at the output of the old and new photodetector circuits, as implemented in GEO 600.
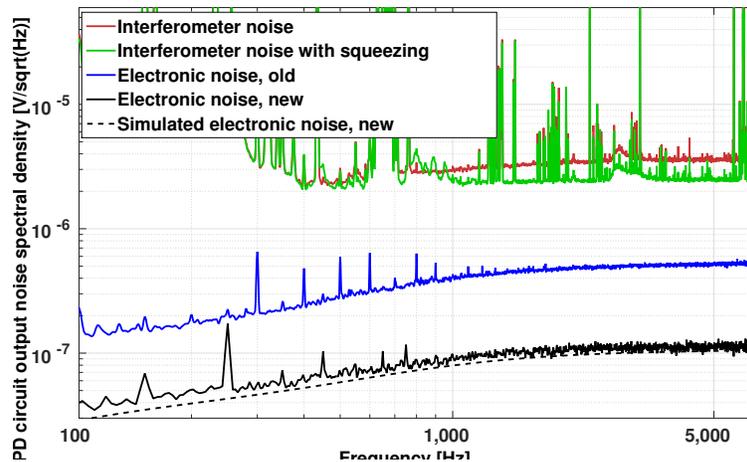
Fig. 7. Output voltage noise spectral densities for different conditions of the GEO 600 interferometer. The red trace shows interferometer noise (mostly shot noise at frequencies above 1 kHz) under normal operating conditions, but without squeezing. The green trace results from application of squeezed states, which is the default operating condition. Both traces were taken with a photocurrent of 6 mA. Also shown are the electronic noise levels of the PD readout circuits (with no light present on the PD) of the old and new photodiode electronics (blue and black, respectively). For all measurements, an attenuation of 3 dB is applied to the output X3 in Fig. 9 before recording the signal. The dashed curve shows the simulated noise of the new circuit, which is the same curve as the total noise in Fig. 5, but also scaled by 3 dB to be comparable to the measured noise.

An improvement of the shot-noise to electronic noise ratio from about a factor of 7 to more than a factor of 30 is observed, corresponding to a total improvement of a bit more than a factor of 4. For the squeezed shot noise the SNR is improved from a factor of 4.5 to a factor of more than 20. The noise equivalent photocurrent (where shot noise equals electronic noise) of the new circuit is about 5 μA with a usable range of 20 mA photocurrent. Since the the new circuit uses only 30 % of its range (6 mA / 20 mA), while the old one used 50 %, the total dynamic range (defined as ratio of maximum DC current to electronic noise) was improved by a factor of 7.

The observed squeezing did improve by about 2.5 % or 0.2 dB with the new circuit as shown in Fig. 8. This corresponds well to the expected improvement in observed squeezing (compare Fig. 1). A circuit based on the new design has been in continuous use at GEO 600 since July 2015 and no negative effects of the new circuit have been observed.

In the future, if higher squeezing levels can be realized at GEO 600 or other detectors, the benefits will be even larger. For example, when aiming for 10 dB of observed squeezing, the signal-to-noise ratio with squeezing and the old detection electronics would be only about a factor of 2, thus reducing the observed squeezing by 1 dB!
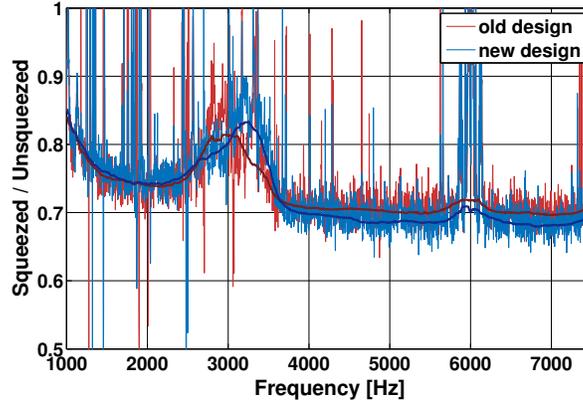
Fig. 8. Spectral ratios of squeezed noise divided by un-squeezed noise for the old and new photodetector designs. With the new design the spectral ratio is lowered by about 2.5 % at frequencies of several kHz, corresponding to an improvement of the observed squeezing level of about 0.2 dB. The irregular structure around 3 kHz is caused by a non-stationary noise feature at the time of the measurements and is not related to the PD circuits under test here.

5. Conclusion

We proposed and experimentally demonstrated a new photodetection circuit design, which allows for an ultra-low noise readout of shot noise in the audio band while detecting photocurrents of up to 20 mA. The dynamic range has been increased by a factor of 7, compared to the formerly used circuit design, thus providing headroom for future laser power increase and higher squeezing levels. The new circuit is in particular useful for squeezed light applications where contribution from electronic noise is critical and for large-scale experiments where even small improvements of the signal-to-noise ratio are worthwhile to pursue. A circuit based on the new design has been in continuous use at GEO 600 since July 2015.

6. Appendix

6.1. Schematic of actual solution

The actual solution finally tested and implemented in GEO 600 is shown in Fig. 9. The new topology proposed in this paper is in the lower left of the diagram, in section C. The series resistor R2 in line with the inductor L2 is used to set the zero of the frequency response together with the copper resistance of coil L2 (24 Ω in this case). Ri sets the pole frequency (together with L2) as mentioned above. In this example, the zero frequency is set to $f_z =$ 3 Hz and the pole frequency to $f_P =$ 100 Hz. The circuitry on the right hand side of section C serves as frequency shaping stage, tailored to subsequent analog-to-digital conversion. It was designed to not affect the SNR (shot noise to electronic noise) significantly. The noise from this stage is dominated by the thermal noise of the impedance of the input network, consisting of R40, R41, and C5. Above 1 kHz the noise of the frequency shaping stage is a factor of 11 lower than the thermal noise of the current-to-voltage conversion resistor, R14, in the previous stage.

Section B shows circuitry providing a radio frequency path for the photocurrent which is used to control the phase of the squeezed light application (with the signal derived from this photodetector) [11]. Inductor L1 provides some isolation at high frequency between sections B and C. It prevents RF photocurrent to significantly enter section C, and prevents noise currents

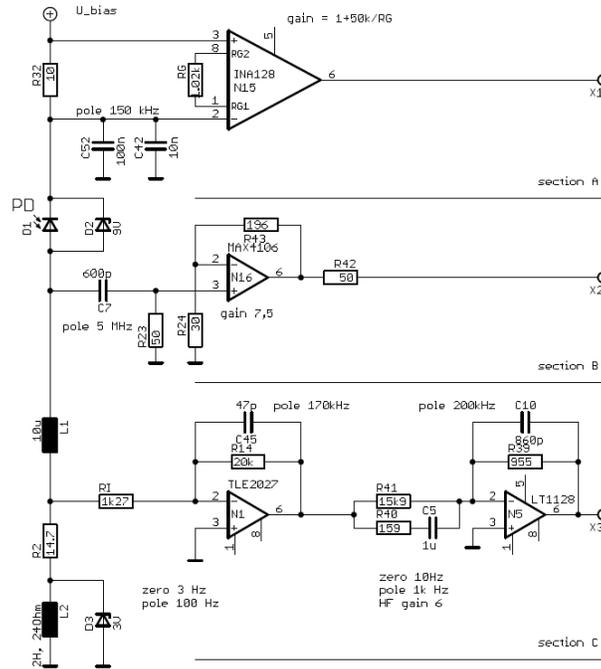of section C to significantly enter section B.

Fig. 9. Simplified actual circuit diagram for the implementation at GEO 600. The proposed new topology is shown on the left side of section C. Section B shows circuitry providing a radio frequency path for the photocurrent which is used to control the phase of the squeezed light application. Section A shows the implementation of a monitor output for the instantaneous photocurrent. While being slightly more complex, this is a clean and frequency independent way to monitor the photocurrent for auxiliary control purposes. The photodiode D1 is an Indium-Gallium-Arsenide type optimised for ultra-high quantum efficiency (typically 99 %). The diameter of D1 is 3 mm and its capacity is approx. 600 pF. Zener diodes D2 protects D1 from too high bias (in case of faults), whereas D3 serves as a shunt for self-induction of L3 in case of rapidly reducing photocurrent.

6.2. Images

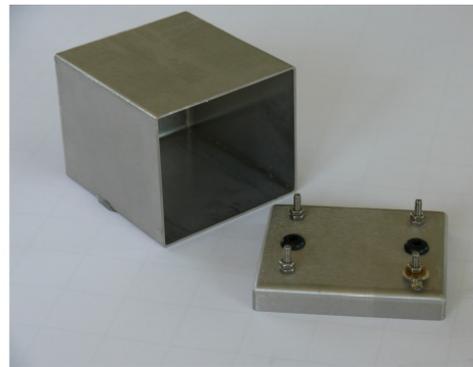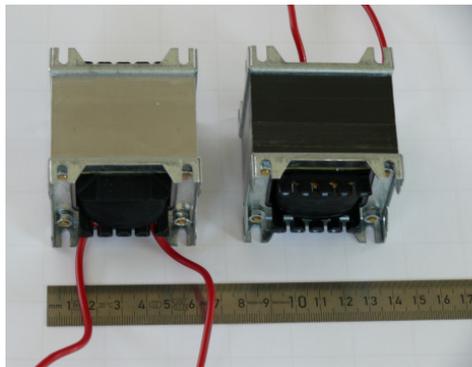The left hand side of Fig. 10 shows images of the two inductors used for the measurements in Fig. 10.

Fig. 10. Left: Images of the two inductors under test, which use different core materials: Mu metal (left), and Silicon/Iron (right). Both inductors have dimensions of 60 x 60 x 55 mm. The layer thickness of the core material is approx. 0.5 mm. Both of these inductors have an inductance of L=2 H and an Ohmic resistance of $24\,\Omega$. The maximum current (avoiding magnetic saturation) is about 20 mA. Right: Image of the Mu metal shield container used as housing for an inductor.